Modeling and Process Simulation of Hollow Fiber Membrane Reactor Systems for Propane Dehydrogenation

Seung-Won Choi, David S. Sholl, and Sankar Nair
School of Chemical & Biomolecular Engineering, Georgia Institute of Technology, Atlanta, GA 30332

Jason S. Moore, Yujun Liu, Ravindra S. Dixit, and John G. Pendergast
Engineering and Process Sciences, The Dow Chemical Company, Freeport, TX 77541

DOI 10.1002/aic.15785
Published online May 18, 2017 in Wiley Online Library (wileyonlinelibrary.com)

We report a detailed modeling analysis of membrane reactor systems for propane dehydrogenation (PDH), by integrating a two-dimensional (2-D) nonisothermal model of a packed bed membrane reactor (PBMR) with ASPEN process simulations for the overall PDH plant including downstream separations processes. PBMRs based on ceramic hollow fiber membranes—with catalyst placement on the shell side—are found to be a viable route, whereas conventional tubular membranes are prohibitively expensive. The overall impact of the PBMR on the PDH plant (e.g., required dimensions, catalyst amount, overall energy use in reaction and downstream separation) is determined. Large savings in overall energy use and catalyst amounts can be achieved with an appropriate configuration of PBMR stages and optimal sweep/feed ratio. Overall, this work determines a viable design of a membrane reactor-based PDH plant and shows the potential for miniaturized hollow-fiber membrane reactors to achieve substantial savings. © 2017 American Institute of Chemical Engineers *AIChE J*, 63: 4519–4531, 2017
Keywords: membrane reactor, propane dehydrogenation, zeolite membrane, process simulation

Introduction

Propylene is an important feedstock for the production of valuable chemical products such as polypropylene and acrylonitrile. Propylene can be produced from steam cracking of naphtha, but there is growing attention to propane dehydrogenation (PDH), which is attractive especially in North America and the Middle East due to their abundant supply of propane.[1,2] PDH systems have been commercialized by CB&I Lummus[3–8] and UOP.[9–15] However, PDH is energy intensive (due to its highly endothermic nature) and thermodynamically limited. Also, the downstream separation of the equilibrium propylene/propane mixture requires even more energy than the reaction step, due to the small volatility difference. The separation is currently achieved in cryogenic or high-pressure distillation columns with more than 100 trays.[16–18] The membrane reactor concept has been proposed for equilibrium-limited reactions like PDH wherein the performance can be intensified by selective permeation of one or more of the products (hydrogen and propylene) through membranes, thereby shifting the equilibrium to the product side.[19–22] Among several different types of membrane reactor configurations the packed bed membrane reactor (PBMR) has been most widely recognized.[21] It consists of a packed bed of catalyst similar to a conventional packed bed reactor (PBR), but with a tubular membrane surrounding the catalyst (Figure 1). It is expected that the enhancement of PDH conversion in PBMR configuration would reduce the separation cost of the downstream separation while increasing propylene production. Membrane reactors have been developed over two decades for other processes such as the water gas shift (WGS) reaction[23–28] and dehydrogenation of alkanes other than propane.[29–32] The literature has generally focused on H_2-selective membranes with large permeabilities to significantly increase the conversion. For example, Kim et al. performed experimental studies of zeolite MFI membrane reactors for high-temperature WGS at different experimental conditions.[23–25] Chein et al. investigated the effect of various sweep gas conditions on the WGS membrane reactor.[28] Ethane dehydrogenation in membrane reactors was examined by Champagnie et al. using Pt-impregnated alumina membranes.[29] Van der Bergh et al. investigated isobutene dehydrogenation in membrane reactors using DDR-type zeolite membranes.[32] Steam reforming reactions in membrane reactors have been studied by several research groups in an effort to increase H_2 production.[33–39] More recently, significant attention has also been paid to the development of membrane reactors for PDH.[40–49] In early studies, Ziaka et al. used ceramic membranes to enhance PDH conversion and selectivity.[40,41] Other groups have studied the use of silica[43,44] and metallic Pd[42,48] membranes. H_2-selective zeolite membrane reactors have also been shown to significantly increase propane conversion while maintaining high selectivity.[50]

There is considerable interest in modeling of membrane reactors to investigate their performance and provide

Additional Supporting Information may be found in the online version of this article.

Correspondence concerning this article should be addressed to S. Nair at sankar.nair@chbe.gatech.edu or D. S. Sholl at david.sholl@chbe.gatech.edu.

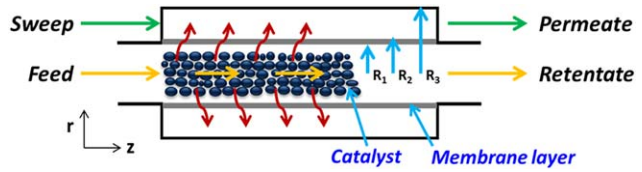

Figure 1. Schematic of a PDH PBMR.

The red arrows denote permeation through the membrane surrounding the packed bed. R_1, R_2, and R_3 denote the membrane inner radius, membrane outer radius, and radius of the shell side respectively. [Color figure can be viewed at wileyonlinelibrary.com]

information for selecting operating configurations and membrane properties. Work in this direction initially focused on applying simple one-dimensional (1-D) isothermal models in different ranges of operating conditions.[46,49] One-dimensional models have also been used for ethylbenzene dehydrogenation, partial oxidation of methane, and ethylene oxidation.[51] Although the 1-D isothermal model does not consider potentially important issues such as mass dispersion or temperature variations, it is still widely applied, especially for laboratory-scale reactors.[52–55] More detailed 2-D and nonisothermal models have also been developed.[47,56–58] For example, Gobina et al. developed a 2-D isothermal model for ethylbenzene dehydrogenation and compared the performances of reactors that used Pd-Ag membranes and microporous ceramic membranes.[57] Koukou used a 2-D isothermal model to evaluate dispersion effects with low and high H_2 permeability membranes for cyclohexane dehydrogenation.[58] In the case of PDH, most work has focused on experimental aspects but a few modeling studies on PBMRs have appeared. For example, Shelepova et al. performed 2-D modeling studies of PDH in PBMR combined with oxidation of hydrogen reaction in permeate side.[47] Recently Choi et al. examined the feasible 'operating windows' using a 1-D PBMR PDH model and investigated the interactions between membrane permeation and catalyst kinetics for selection of material properties and reactor configurations.[49] The effect of countercurrent sweep gas configurations has also been studied by modeling and experiment.[28,49,56,58–61] Although countercurrent operation may increase the product permeation driving force, Choi et al. showed that it is beneficial only in a limited range of operating conditions and at low weight-hourly space velocity (WHSV).[49]

No work has been reported in the literature on modeling of scaled-up PBMR systems integrated with downstream separation processes such as sweep gas removal and the C_3 splitter for separation of propylene from propane. Such a model is important for understanding the overall operation and viability of chemical production processes that incorporate a membrane reactor system. In this article, we develop a process-level modeling analysis of a PDH process incorporating a PBMR and downstream separation units. Several new features are introduced at both the reactor and process levels. At the reactor level, we describe the PBMR system using a detailed 2-D nonisothermal model to examine mass dispersion effects and the temperature drop in the endothermic PDH reaction. The model also examines the effects of the high-temperature sweep gas in a series of reactors with interstage heaters. We address the issue of PBMR scalability by comparing the use of conventional tubular membranes to hollow fiber membranes. The required PBMR size is calculated for a target propylene production, and better configurations are considered to overcome the limitations of conventional PBRs. At the process level, simulations using a flowsheeting package such as ASPEN can be a valuable tool for understanding the impact of the PBMR on the overall process and guiding industrial process design. Here, we have overcome the technical challenge of incorporating a membrane reactor model into ASPEN. Specifically, we incorporate the 2-D PBMR PDH model into an ASPEN–FORTRAN simulation that includes downstream separation units. This allows us to determine the advantages of using a PBMR system in a PDH plant. In particular, we compare the energy loads of PBR and PBMR systems and elucidate the effect of PDH conversion and selectivity enhancements on the downstream separation energy load, thus providing design guidelines for PBMR incorporation in a commercial-scale PDH plant.

Modeling Methods

Nonisothermal 2-D PBMR modeling

The 2-D governing mass transport equations (each with accompanying boundary conditions) are:

$$\frac{\partial(u_T C_i^t)}{\partial z} = D_t\left\{\frac{1}{r_t}\frac{\partial}{\partial r_t}\left(r_t\frac{\partial C_i^t}{\partial r_t}\right)\right\} + \rho_B(-r_A) \text{ (Tube side)} \tag{1a}$$

$$\left[\begin{array}{l} z = 0\,, \quad C_i = C_{i0}{}^t\,, \quad r_t = 0\,, \quad \dfrac{\partial C_i^t}{\partial r_t} = 0\,, \\ r_t = R_1\,, \quad D_t\dfrac{\partial C_i^t}{\partial r_t} = -q_i(P_i^t - P_i^m) \end{array}\right] \tag{1b}$$

$$D_m\frac{1}{r_m}\frac{\partial}{\partial r_m}\left(r_m\frac{\partial C_i^m}{\partial r_m}\right) = 0 \text{ (Inside membrane support)} \tag{2a}$$

$$\left[\begin{array}{l} r_m = R_1\,, \quad D_m\dfrac{\partial C_i^m}{\partial r_m} = -q_i(P_i^t - P_i^m) \\ r_m = R_2\,, \quad D_m\dfrac{\partial C_i^m}{\partial r_m} = D_s\dfrac{\partial C_i^s}{\partial r_s} \end{array}\right] \tag{2b}$$

$$\frac{\partial(u_s C_i^s)}{\partial z} = D_s\left\{\frac{1}{r_s}\frac{\partial}{\partial r_s}\left(r_s\frac{\partial(u_s C_i^s)}{\partial r_s}\right)\right\} \text{ (Shell side)} \tag{3a}$$

$$\left[\begin{array}{l} z = 0\,, \quad C_i = C_{i0}{}^s \\ r = R_2\,, \quad D_s\dfrac{\partial C_i^m}{\partial r_s} = D_m\dfrac{\partial C_i^s}{\partial r_s} \\ r = R_3\,, \quad D_s\dfrac{\partial C_i^s}{\partial r_s} = 0 \end{array}\right] \tag{3b}$$

Here, D is the dispersion coefficient, u is the linear velocity of convective flow at the tube and shell side based on a plug flow assumption, and R_1, R_2, and R_3 are the membrane tube inner surface radius, membrane tube outer surface radius, and the shell/jacket radius, respectively. Superscripts and subscripts t, m, and s denote the tube, membrane support and shell side, respectively. The membrane layer is located on the inner surface of the tube. C and q are concentration and membrane permeance of each component i, ρ_B is the bulk density of catalyst in the packed bed and r_A represents the reaction kinetics. We used the following kinetic expression:

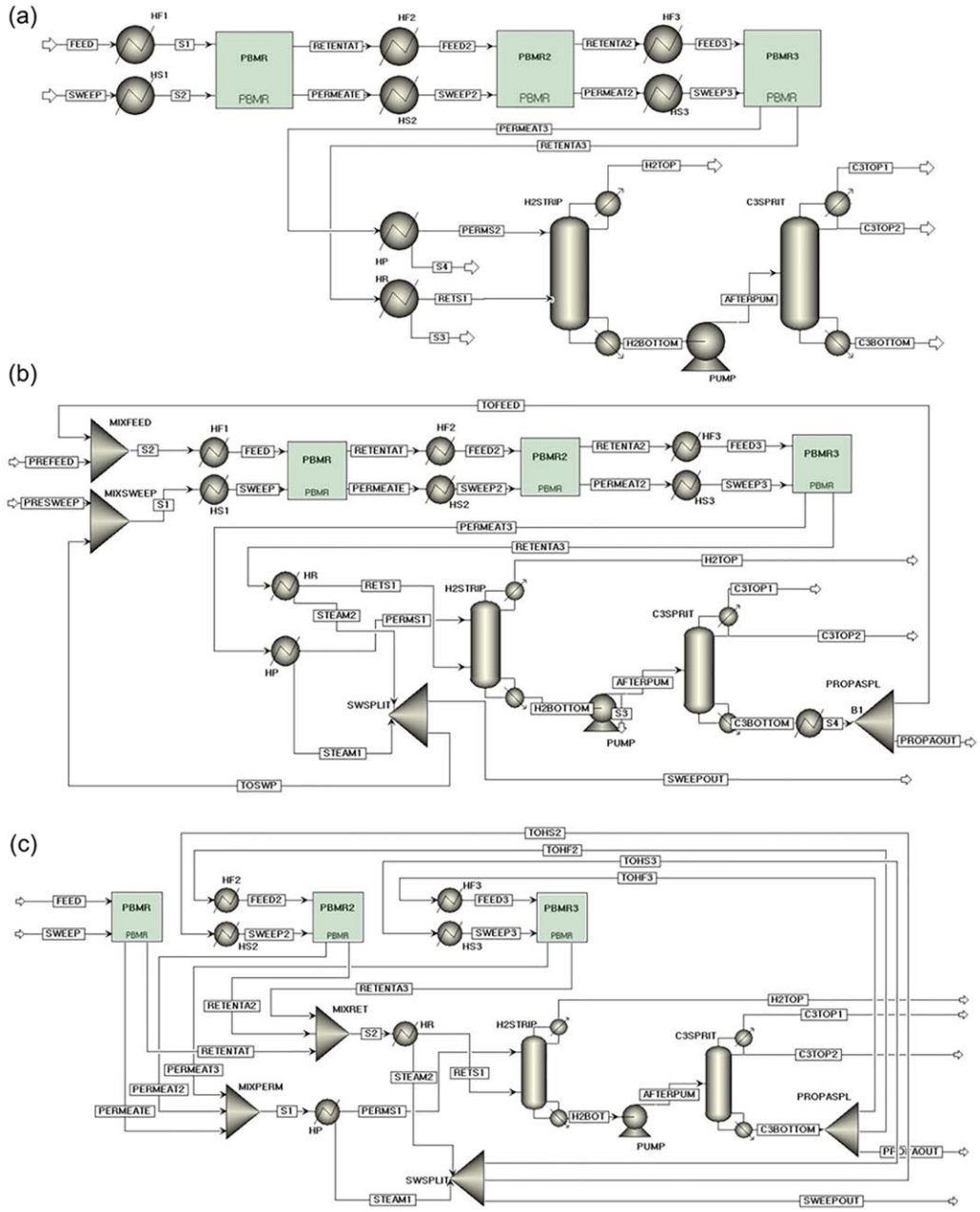

Figure 2. ASPEN flowsheets of PDH plant using 2-D nonisothermal PBMR model with downstream separation: (a) single-pass, (b) simple recycle, (c) recycle with reactor stages in parallel and recycled propane distributed equally to the second and third stages.

[Color figure can be viewed at wileyonlinelibrary.com]

$$r_A = \frac{k_1\left(P_A - P_B P_C/K_{eq}\right)}{1+K_{a2}P_B} \tag{4a}$$

$$\left(\begin{array}{l} k_1 = k_1{}^0 \exp\left(\dfrac{-E_a}{R_g}\left(\dfrac{1}{T} - \dfrac{1}{T_0}\right)\right) \\ K_{a2} = K_{a2}{}^0 \exp\left(\dfrac{-\Delta H_a}{R_g}\left(\dfrac{1}{T} - \dfrac{1}{T_0}\right)\right) \end{array}\right) \quad (T_0 = 873\ \text{K}) \tag{4b}$$

Here, k_1 is the forward reaction rate (mol s^{-1} m^{-2} Pa^{-1}), K_{eq} is the temperature dependent reaction equilibrium constant (kPa), K_{a2} is the equilibrium constant for adsorption of propylene on the surface (kPa^{-1}), and P_a, P_b, P_c are the partial pressures of propane, propylene, and hydrogen, respectively (kPa). The parameters in Eqs. 4a, b were obtained by fitting the kinetic model to detailed PDH measurements carried out in a quartz-tube reactor with a Na-doped Cr_2O_3/Al_2O_3 catalyst (supplied by Dow Chemical). The Supporting Information contains full experimental details, data, and fitting results. Supporting Information Table S1 lists the values of the fitted parameters used in this work. In comparison to the 1-D model discussed in our previous work,[49] here we have replaced the membrane permeation term with a dispersion term to describe the radial concentration profile inside the tube. The membrane permeance is then included in the boundary conditions for the tube-side and membrane support (Eqs. 1b and 2b). In the 1-D

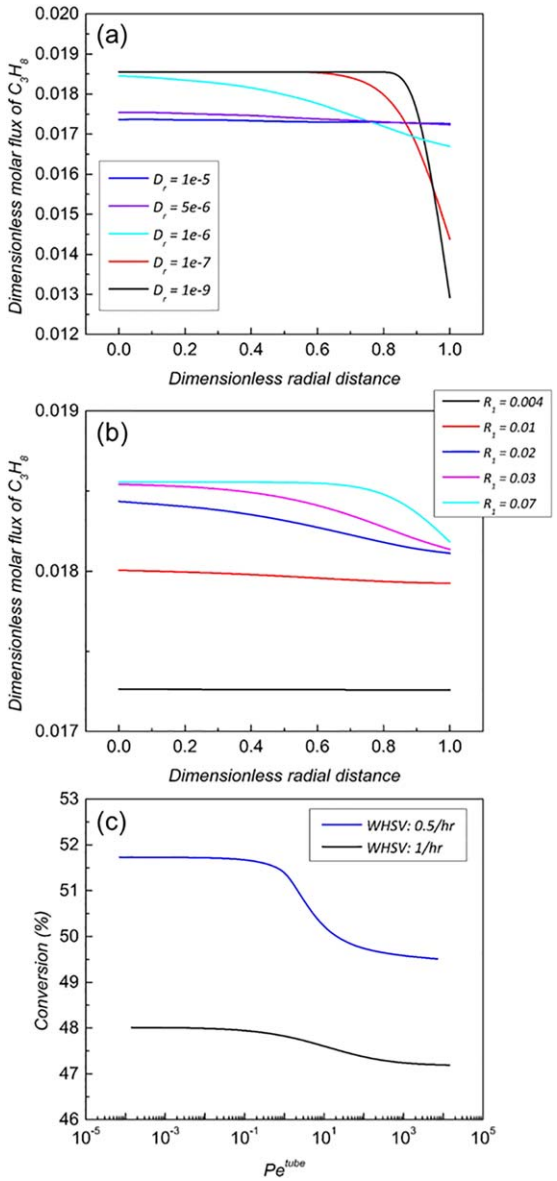

Figure 3. (a) Effect of dispersion coefficient (D_t, $m^2\ s^{-1}$) on dimensionless axial molar flux rate of C_3H_8, (b) effect of tube radius (R_1, m) on dimensionless axial molar flow rate of C_3H_8, and (c) relation between Pe_{tube} and conversion (%).

[Color figure can be viewed at wileyonlinelibrary.com]

model, the dimensionless quantity Pe_{mem} represents the ratio of convective transport and membrane diffusive transport rates.[49] Similarly, the Pe_{mem} can be defined in the 2-D model as follows:

$$\mathrm{Pe_{mem}} = \frac{u_{T0}}{q_{H_2} R_g T} \frac{R_1}{2L} \tag{5}$$

Here u_{T0} is the linear velocity of the feed flow rate ($m\ s^{-1}$) at the tube side, and L is the reactor length. In addition, the 2-D model defines a second dimensionless number Pe_{tube} which is the ratio of convective and radial transport rates at the tube side, to assess mass dispersion effects in the packed bed:

$$Pe_{\mathrm{tube}} = \frac{u_{T0}/L}{D_t/R_1{}^2} \tag{6}$$

When Pe_{tube} increases, the convective transport from feed flow dominates the system and the membrane transport will only affect the vicinity of the membrane surface. Therefore, increasing the effect of convective transport leads to a decrease in membrane permeation and PBMR performance. When the Pe_{tube} decreases, membrane transport will be important throughout the radial coordinate. As $Pe_{tube} \to 0$, the system approaches the 1-D model. In a scaled-up system, the temperature distribution cannot be neglected, for example, the adiabatic temperature drop along the axial direction. Hence, nonisothermal modeling is required to provide a more accurate PBMR design. We use 2-D nonisothermal energy balance equations for adiabatic reactors with radial heat conduction. The energy balance equations and boundary conditions are as follows:

$$\frac{\partial(u_T \rho_T C_p \mathrm{T}_t)}{\partial z} = k_{eff}\left\{\frac{1}{r_t}\frac{\partial}{\partial r_t}\left(r_t \frac{\partial \mathrm{T}_t}{\partial r_t}\right)\right\} + \rho_B(-\mathrm{r_A})(-\Delta H) \quad \text{(Tube side)} \tag{7a}$$

$$\begin{bmatrix} z = 0\ , & \mathrm{T}_t = \mathrm{T}_{t0} \\ r_t = 0\ , & \dfrac{\partial \mathrm{T}_t}{\partial r_t} = 0 \\ r_t = \mathrm{R}_1\ , & k_{\mathrm{eff}} \dfrac{\partial \mathrm{T}_t}{\partial r_t} = \mathrm{h}_T(\mathrm{T}_m - \mathrm{T}_t) \end{bmatrix} \tag{7b}$$

$$\frac{1}{r_m}\frac{\partial}{\partial r_m}\left(r_m \frac{\partial \mathrm{T}_m}{\partial r_m}\right) = 0 \quad \text{(Inside membrane support)} \tag{8a}$$

$$\begin{bmatrix} r_m = \mathrm{R}_1\ , & k_m \dfrac{\partial \mathrm{T}_m}{\partial r_m} = \mathrm{h}_T(\mathrm{T}_m - \mathrm{T}_t) \\ r_m = \mathrm{R}_2\ , & k_m \dfrac{\partial \mathrm{T}_m}{\partial r_m} = \mathrm{h}_S(\mathrm{T}_s - \mathrm{T}_m) \end{bmatrix} \tag{8b}$$

$$\frac{\partial(u_S \rho_S C_S \mathrm{T}_s)}{\partial z} = k_{\mathrm{gas}}\left\{\frac{1}{r_s}\frac{\partial}{\partial r_s}\left(r_s \frac{\partial \mathrm{T}_s}{\partial r_s}\right)\right\} \quad \text{(Shell side)} \tag{9a}$$

$$\begin{bmatrix} z = 0\ , & \mathrm{T}_s = \mathrm{T}_{s0} \\ r_s = \mathrm{R}_2\ , & k_{\mathrm{gas}} \dfrac{\partial \mathrm{T}_s}{\partial r_s} = \mathrm{h}_s(\mathrm{T}_s - \mathrm{T}_m) \\ r_s = \mathrm{R}_3\ , & k_{\mathrm{gas}} \dfrac{\partial \mathrm{T}_s}{\partial r_s} = \mathrm{h}_w(\mathrm{T}_w - \mathrm{T}_s) \end{bmatrix} \tag{9b}$$

Here, T represents temperature, k_{eff} is the effective thermal conductivity of the packed bed, k_{gas} is thermal conductivity of sweep gas, ρ and C_p are the average density and heat capacity, respectively, and h is the heat-transfer coefficient. The coupled mass and heat-transfer equations are solved simultaneously along the radial and axial directions. We apply the same heat-transfer parameters as used in Choi et al.[49] To solve the equations, we apply finite difference methods (FDM) using central differencing scheme for the radial direction and backward differencing scheme for the axial direction. We solve for the radial concentration and temperature profiles, and then the concentrations, flow rates and temperature profiles are updated at each axial position.

PDH flowsheet and ASPEN–FORTRAN modeling

To incorporate the reactor model into an ASPEN process simulation, the membrane reactor simulation module (written in

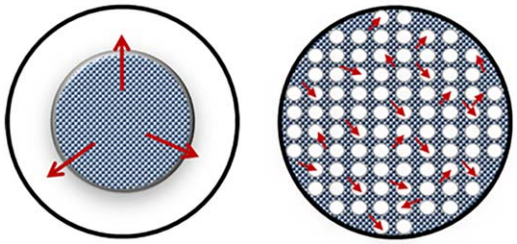

Figure 4. Schematic of PBMR configuration using a tubular membrane with packed catalyst in the bore side (left), and a hollow fiber membrane bundle with catalyst on the shell side (right). The shaded areas and arrows represent packed catalyst and the direction of gas permeation (from the catalyst toward the tube/fiber surface), respectively.

[Color figure can be viewed at wileyonlinelibrary.com]

FORTRAN) was first prepared for reading input parameters, calculating the reactor performance, and generating output results. This was done by creating a PBMR model block and then using the ASPEN subroutine "usrus2.f" that allows integration of user-supplied system models with the process simulator. We thus obtain a customized PDH process simulator incorporating the 2-D nonisothermal PBMR model. The PBMR PDH plant flowsheet is shown in Figure 2. The simulator does not include deactivation behavior of current PDH catalysts at high temperature. We assume that the calculated PDH conversion is the same as the initial value in the real PDH process before the catalyst becomes highly deactivated. This assumption is reasonable considering that the maximum conversion can be always maintained in commercial PDH processes by regeneration cycles such as continuous catalytic regeneration (CCR) in the UOP process or use of parallel reactors in Catofin process.[2] The input parameters for the PBMR block are reactor dimensions, feed/sweep flow rates, kinetic parameters for PDH reaction, and the membrane properties such as permeance and selectivity. We consider three adiabatic PBMRs in series with interstage heaters with or without a recycle loop (Figures 2a, b). We also consider a second type of configuration with the reactor stages in parallel and with the recycled propane distributed between the second and third stage (Figure 2c). The overall feed flow rate is 4000 kmol h^{-1} for the single-pass (no recycle) system, which corresponds to about 550 kTA (kilotons per annum) propylene production in a typical PDH plant if 40% propane conversion is assumed. Hence, for the recycle configurations which have an overall conversion of 100%, we use 2000 kmol h^{-1} for a similar production rate. For downstream H_2 separation, we use a distillation column with 10 equilibrium stages and reflux ratios in the range of 1.5–5. Pressure swing adsorption can also be used.[62–64] A distillation column is used as the downstream C_3 splitter, with 200 equilibrium stages and large reflux ratios (30–70, depending on the feed composition).

Results and Discussion

Effect of dispersion and membrane radius in the isothermal model

As the radial dispersion coefficient (D_t, m^2 s^{-1}) and the tube radius (R_1, m) determine the value of Pe_{tube} (Eq. 6), we first clarify the effect of these parameters on the dimensionless axial molar flow rate of propane at the tube outlet. The dimensionless axial molar flux of each component i can be defined by a molar flux divided by the total feed flux as follows:

$$\tilde{u}_i = \frac{u_t C_i}{u_{T0} C_{T0}} \tag{10}$$

The total feed flux is defined by the linear feed velocity ($U_{T0,}$ m s^{-1}) multiplied by the total feed concentration ($C_{T0,}$ mol m^{-3}). Similarly, the dimensionless radial distance at the tube side is

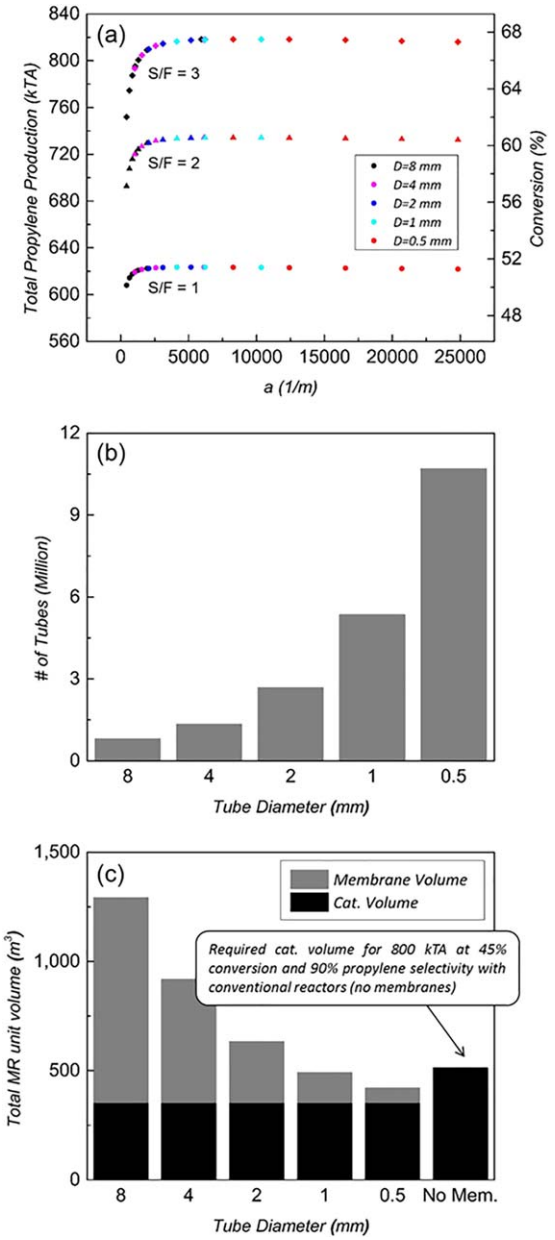

Figure 5. (a) Propylene production rate and conversion as a function of membrane surface area per unit volume, *a*. (b) Comparison of required number of membrane tubes for different target conversions (or propylene production rates) with a fixed 4000 kmol h^{-1} propane feed. (c) Comparison of required membrane reactor volume for 800 kTA propylene production (S/F = 3).

[Color figure can be viewed at wileyonlinelibrary.com]

Table 1. PBMR Configuration for 800 kTA of Propylene Production at S/F = 3

Membrane diameter (mm)	0.5
Membrane thickness (mm)	0.125
Catalyst volume (shell volume, m^3)	350
Catalyst amount (ton)	525
Feed flow rate (kmol h^{-1})	4000
Preheat temperature (°C)	650
WHSV (h^{-1})	0.34
Total membrane reactor volume (m^3)	421

defined by a radial position divided by tube radius (R_l). We assume a membrane with H_2 permeance of 1×10^{-7} mol s^{-1} m^{-2} Pa^{-1} and perfect H_2 selectivity. A zeolite SAPO-34 (~0.38 nm pore size) membrane is one example approximating these characteristics, with H_2 permeances up to 3×10^{-7} mol s^{-1} m^{-2} Pa^{-1} and H_2/C_3 selectivities > 20.[21,50] The decrease in axial propane flux near the membrane circumference (Figure 3a) is due to increased PDH resulting from H_2 removal by the membrane. At low D_t, the propane flux profile is dominated by bulk convection. The effect of increased PDH is only seen in the vicinity of the membrane. As D_t increases (i.e., Pe_{tube} decreases), the effect of the membrane is felt throughout the radial coordinate and lower axial fluxes are seen throughout the tube cross-section. In Figure 3b, we plot the dimensionless axial molar flux of propane at the reactor exit for different tube radii, at fixed $D_t = 5 \times 10^{-5}$ m^2 s^{-1}. Decreasing the tube radius (i.e., Pe_{tube} decreases) leads to lower fluxes throughout the cross-section. In general, it is clear that a lower Pe_{tube} is required for membrane permeation to play an important role. Hence, a longer membrane of smaller radius is a better candidate for PDH PBMR applications. Figure 3c shows the PDH conversion versus Pe_{tube} for two weight hourly space velocities (WHSV, mass flow rate divided by the amount of catalyst, h^{-1}). A lower Pe_{tube} is required for increased conversion which approaches a plateau as $Pe_{tube} < 0.1$. The other Péclet number Pe_{mem} (Eq. 5) is proportional to the ratio of catalyst volume and membrane surface area. Hence, as in the case of Pe_{tube}, higher conversion enhancement (due to a larger surface area for membrane permeation) is expected with lower Pe_{mem} assuming that the catalyst volume is sufficient to reach at least the equilibrium conversion.

Scale-up of PDH PBMR with hollow fibers

The PBMR configuration reported in the literature generally consists of a membrane tube containing a packed catalyst and a sweep gas on the shell side (Figure 1). The tubes are generally macroporous ceramic tubes (e.g., 8 mm ID) with a thin H_2-selective membrane grown or deposited on the inner surfaces. The use of tubes with relatively large diameter leads to a large reactor volume due to the low membrane surface area available per unit volume. Hence, we suggest the use of closely packed hollow fiber membranes[65–71] for scale-up of PDH PBMRs (Figure 4). Ceramic (e.g., α-alumina) hollow fibers of ODs as small as 1 mm can be fabricated by spinning processes and used for deposition/growth of membranes.[72–74] It is neither feasible to pack the catalyst into hollow fibers (due to their much smaller diameters), nor is it desirable (due to the difficulty of removing the catalyst for replacement or regeneration). Instead, the packed catalyst would be placed on the shell side with the array of hollow fiber membranes embedded in it. The membranes could be located on the outer surfaces of the fibers, and the H_2-rich permeate would be collected on the bore side of the fibers.

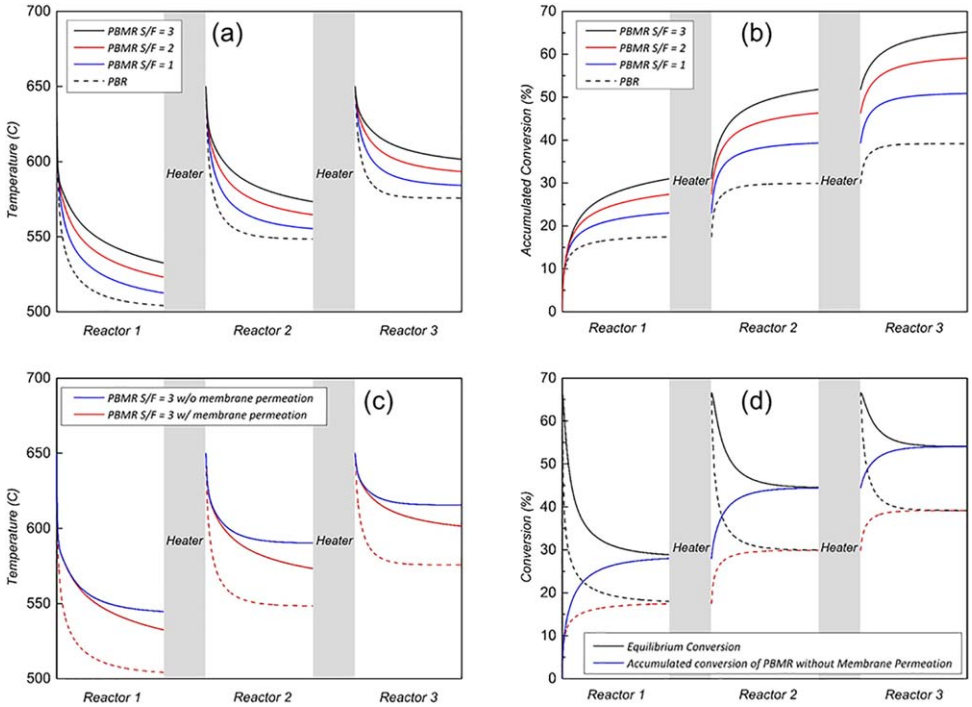

Figure 6. (a) Temperature profiles and (b) accumulated conversion of three reactor stages (Reactor 1, Reactor 2, Reactor 3) for PBR and PBMR conditions. (c) Temperature profiles of PBMR with and without membrane permeation (S/F = 3). The dashed lines indicate the profiles of PBR. (d) Equilibrium and accumulated conversions along the three reactors using PBMR configuration without membrane permeation (S/F = 3). The dashed lines indicate the equilibrium and accumulated conversions of the PBR.

[Color figure can be viewed at wileyonlinelibrary.com]

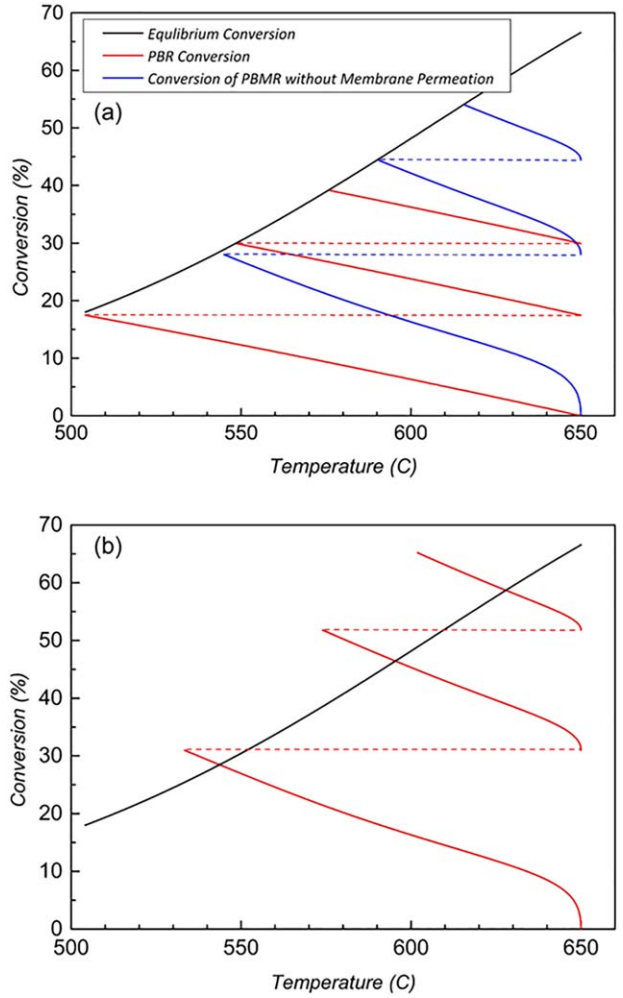

Figure 7. (a) Adiabatic operating line of PBR and zero-permeance PBMR configuration (S/F = 3). (b) Adiabatic operating line of PBMR (S/F = 3) along the three reactors. The dashed lines depict the reheating of retentate streams in interstage heaters.

[Color figure can be viewed at wileyonlinelibrary.com]

We now examine the PDH performance as a function of the dimensions of the membrane tubes in the array, ranging from conventional ceramic tubes (8 mm OD) to hollow fibers (0.5 mm OD). The nonisothermal model is used for this analysis. The propane feed flow rate is fixed at 4000 kmol h^{-1} corresponding to 550 kTA (kilotons per annum) of propylene production in a conventional PDH process (such as Oleflex) with approximately 45% conversion and 90% propylene selectivity.[2] We assume a H_2-selective membrane (permeance of 3 $\times$ 10^{-7} mol s^{-1} m^{-2} Pa^{-1} at the temperature range of operation and assumed that other components such as propane, propylene, and sweep gas have low permeances ($\sim 10^{-10}$ mol s^{-1} m^{-2} Pa^{-1}). When different numbers and sizes of tubes/fibers are considered, the distance between the tubes is adjusted to have a fixed WHSV, and hence the amount of catalyst remains constant. We assume use of steam as a sweep gas as it is abundant in a typical petrochemical plant and can be easily separated by condensation. The sweep/feed molar ratio (S/F) is varied from 1 to 3. We assume that the tubes are uniformly packed, and that the feed, sweep, and catalyst are evenly distributed. It is also assumed that there is negligible heterogeneity in composition and temperature in the spaces between the tubes on the shell side. This assumption is valid if the radial $Pe_{\text{tube}} \ll$ axial Pe_{tube}.[49] For the PBMR configuration using the hollow fibers with $R_1/L \sim 0.01$ as considered here, the effects of radial dispersion are small enough (Figure 3) to validate the assumption (Pe_{tube} is in the order of 10^{-1} or less, depending on the membrane size, while axial Pe_{tube} is more than $\sim 10^6$). Finally, the heat-transfer Péclet number ($\alpha/U_{T0}L$, α is the thermal diffusivity) is very large ($\sim$10,000) in this system, and therefore the radial temperature distribution and axial heat conduction will be negligibly small. As a result of the above assumptions, we can perform calculations on a single tube or fiber and simply multiply by the total number of tubes to obtain the total output of the system.

We begin by calculating the PDH performance using a system of three adiabatic PBMR stages with interstage heaters. Each reactor has 5 m total length. The inlet temperature of both the feed and sweep gases is 650°C and the outlet streams are reheated by the interstage heaters to compensate for the temperature drop occurring during the endothermic reaction. We define a membrane packing density value a (m^{-1}) as follows

$$a = \frac{\text{membrane surface area}}{\text{catalytic volume}} = \frac{2R_2}{(R_3{}^2 - R_2{}^2)(1-\varepsilon)\rho_{\text{cat}}} \quad (11)$$

Here, R_2 represents the radius of membrane tube, R_3 denotes the shell radius which is adjusted for each size of the membrane as mentioned. The quantities $\varepsilon = 0.5$ and $\rho_{\text{cat}} = 3.95$ g cm^{-3} are the void fraction and density of the catalyst (mainly alumina support), respectively. The smaller the membrane radius, the larger is the a value that can be achieved. Pe_{mem} is linearly proportional to a at fixed WHSV, and therefore more effective membrane permeation occurs at larger a values. Figure 5a shows the conversion and corresponding propylene production rate as a function of a with the individual membrane tube diameter and S/F ratio as parameters. Although each diameter setting predicts a different range of PDH performance, the data can be overlapped on the same plot as a function of a at each fixed S/F ratio. Clearly, hollow fiber membranes (0.5–1 mm ID) enable higher conversion at any given S/F ratio due to the large a values that result in faster removal of H_2. Figure 5a also shows that the enhancement of PDH performance reaches a plateau at large a values, which means that very large membrane surface areas (i.e., very thin hollow fibers) do not provide additional benefit. Based upon the propylene output of a single tube/fiber, we can calculate the total number of tubes/fibers required (Figure 5b) for different propylene production levels given a fixed 4000 kmol h^{-1} propane feed rate. At each S/F ratio the target production level is assumed to be located at the onset of the plateau region in Figure 5a, for example, $\sim$800 kTA at S/F = 3. Figure 5c shows the required total volume of the PBMR required for 800 kTA production (i.e., 66% conversion) at S/F = 3). The total PBMR volume is expressed as a summation of the fixed catalytic volume and the total membrane tube/fiber volume. The use of conventional membrane tubes is not feasible for PDH as it leads to a prohibitively large reactor volume (mainly due to the membrane volume). Conversely, the use of hollow fiber membranes is attractive as it requires only a marginal (<15%) additional membrane volume over the fixed volume of catalyst, while boosting propylene production from 550 to 800 kTA. In comparison, a large (40–50%) increase in catalyst volume would be required to achieve the same production increase if a conventional process is to be used. Table 1 lists

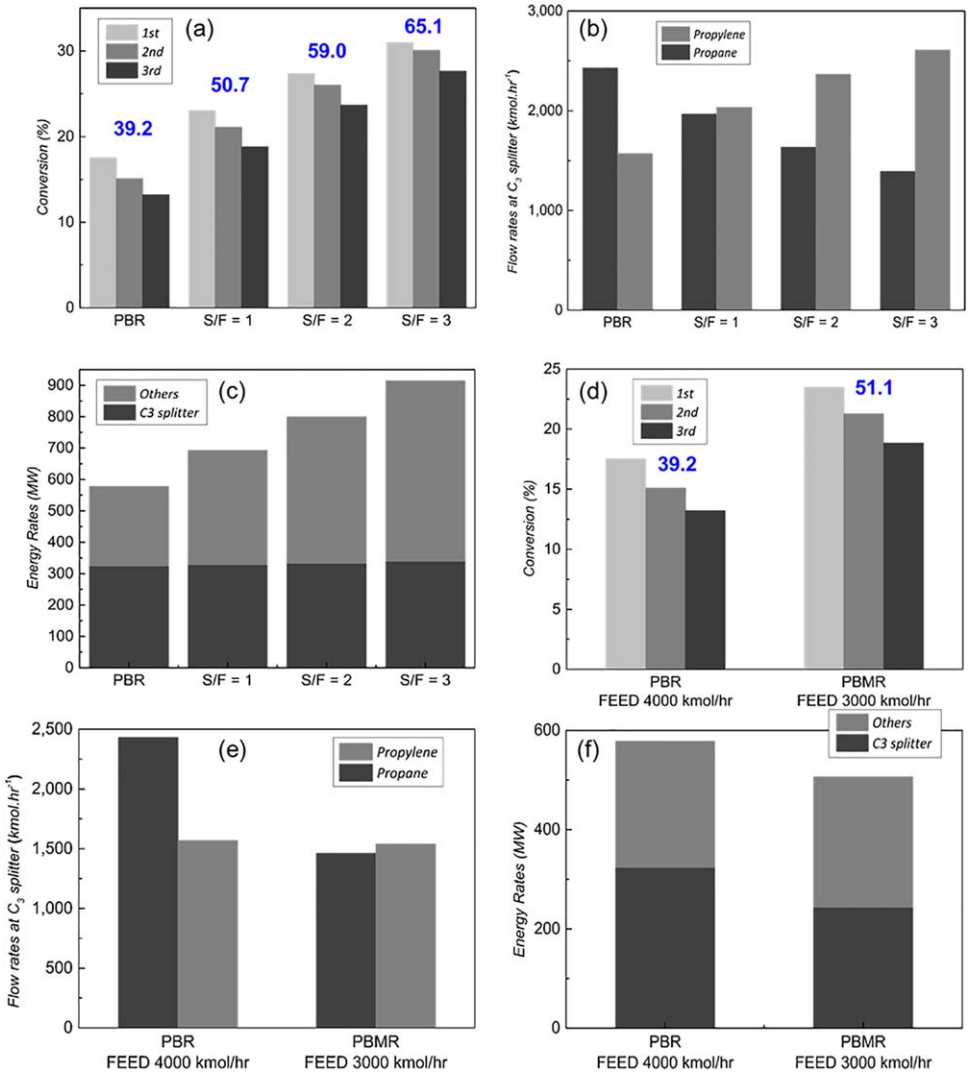

Figure 8. (a) PDH conversions of three-stage PBRs and PBMRs at different S/F. The numerical labels indicate overall conversions. (b) Flow rates of propane and propylene at C_3 splitter entrance and (c) energy duties in PBR and PBMR operation. (d) Conversions of three reactors in a PBR (4000 kmol h^{-1} feed) and PBMR (S/F = 1, 3000 kmol h^{-1} feed). The numerical labels indicate overall conversions. (e) Flow rates of propane and propylene at splitter entrance and (f) energy duties in PBR (4000 kmol h^{-1} feed) and PBMR operation (S/F = 1, 3000 kmol h^{-1} feed).

[Color figure can be viewed at wileyonlinelibrary.com]

the PBMR parameters for this case with hollow fiber membranes of radius 0.25 mm (ID 0.5 mm).

Temperature profiles in hollow fiber PBMRs

Figure 6a shows a comparison of the catalytic side (i.e., shell side) temperature profile of the hollow fiber PBMR (Table 1) with that of the corresponding PBR that uses the same 2-D adiabatic reaction zones with interstage heaters. The presence of the heated sweep gas on the permeate side (i.e., inside the hollow fiber tubes) allows heat transfer into the catalytic side and hence a lower endothermic temperature drop (Figure 6a) and higher conversion (Figure 6b) in each reactor. By dropping the S/F value to 2, we observe a larger temperature drop in the reactors and a drop-in conversion, illustrating the importance of the heated sweep gas. To study this aspect independently of the conversion enhancement by membrane permeation, Figures 6c, d show the temperature profiles and accumulated conversions for a PBMR containing *impermeable* hollow fibers (i.e., no H_2 removal from the catalytic side). For comparison, the results of Figures 6a, b (PBMR with membrane permeation, and conventional PBR with no hollow fibers) are also shown. It is clear that the heat exchange effect of the sweep gas plays a significant role in maintaining a high temperature, and the effect of membrane permeation is critical to achieve conversions much higher than the equilibrium value. For both the PBR and "zero-permeance" PBMR, equilibrium-limited conditions were reached at the end of each reactor stage (Figure 6d). The adiabatic operating lines (Figure 7) can also be used to summarize the temperature-conversion behavior. Moderately higher conversions than the PBR are possible even with the zero-permeance PBMR (Figure 7a) due to heat transfer from the sweep gas, but the equilibrium line is still followed. Further significant enhancements (by breaking the equilibrium limitations) can only be achieved with membrane permeation (Figure 7b).

PDH plant simulation with hollow fiber PBMR

Having established that hollow fiber PBMRs allow large increases in PDH conversion and more efficient heat exchange

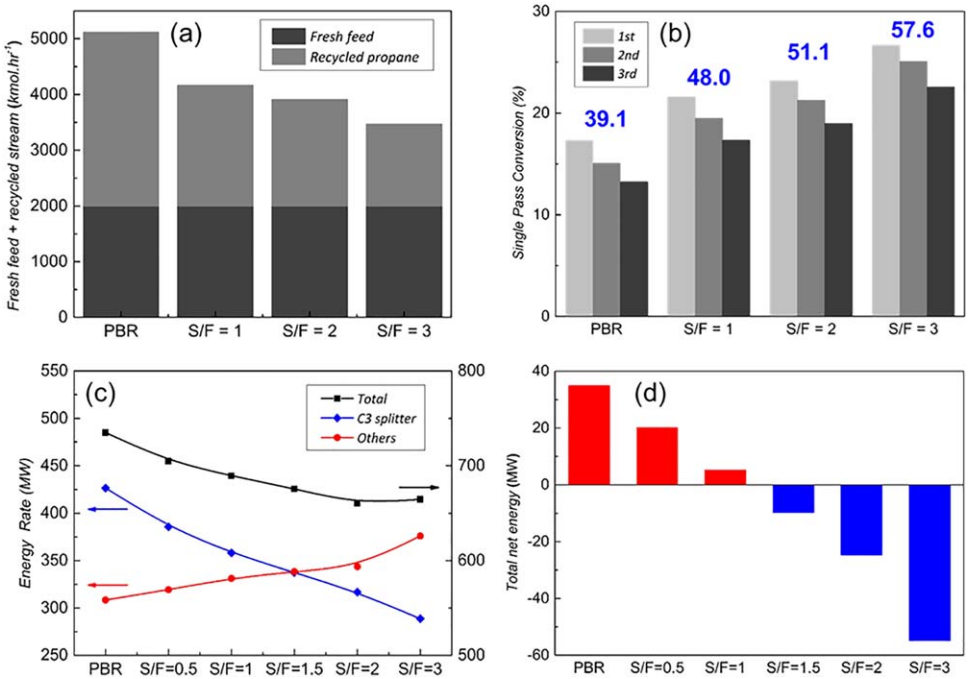

Figure 9. (a) Total flow rates entering PBR and PBMR reactor stages at steady state. (b) Single-pass conversions of each reactor stage in simple recycled PDH plant. The numbers in each condition indicate the overall single-pass conversion. (c) Required energy duties of C_3 splitter, other streams, and total streams with respect to S/F ratios. Solid lines are a guide to the eye. (d) Total net energy duty in PBR and PBMRs.

[Color figure can be viewed at wileyonlinelibrary.com]

with small or moderate increase in the reactor volume, we now examine how these enhancements of PDH performance affect the downstream separation processes and the overall PDH plant. The plant flowsheet is as shown in Figures 2a–c, comprising three cases that are discussed here. The first two cases contain the same PBMR configuration (i.e., three reactor stages in series with interstage heating), with the parameters in Table 1. In regard to downstream separation, we focus on the C_3 splitter which is one of the most energy intensive separation processes in the chemical industry.[16–18] The preheating, reheating, and cooling of outlet streams are also considered.

We first consider the "no-recycle" case of Figure 2a. The key results of the ASPEN simulations are shown in Figures 8a–f. The three PBMR stages are operated in a series arrangement. In Figure 8a, the large enhancements in conversion are clearly seen especially at higher S/F ratios. This significantly alters the relative flow rates of propylene and propane at the C_3 splitter inlet (Figure 8b), ranging from a propylene-lean stream (39.2 mol %) for the PBR to a propylene-rich stream (65.2 mol%) for the PBMR with S/F = 3. Figure 8c compares the total energy duty for PBR and PBMR systems. The energy duty for the C_3 splitter was calculated by simple summation of absolute values of heating and cooling duty of the distillation column. The distillate flow rate and reflux ratio were adjusted for a target of 99.9% purity propylene distillate at each condition. Even though the compositions of the C_3 splitter feed are quite different, the energy duties are not much different as they are generally proportional to the product of the reflux ratio and the distillate rate. Although, a lower reflux ratio can be used at the splitter in the case of PBMRs with higher S/F (due to higher propylene content in the splitter feed), the increased flow rate of propylene in the splitter feed also results in a higher distillation rate. Heat pumping/heat integration of the splitter was not considered here, with the rationale that its effect would be similar in all the cases. In addition to the C_3 splitter, other energy duties are also shown in Figure 8c, which include preheating and reheating of inlet streams, cooling of outlet streams, and the energy duty of the H_2 separation column.

These results highlight an important issue in PDH PBMR applications. Although conversion enhancements can be made by using higher S/F rates, this also requires more energy for heating the sweep and permeate streams and for removal of the sweep gas from the H_2-rich permeate. Therefore the "no-recycle" PBMR increases both propylene production and total energy load. For a more direct comparison between the PBR and PBMR, we adjusted the feed flow rate at the PBMR inlet to 3000 kmol h^{-1} to obtain the same propylene production (1500 kmol h^{-1}) as the PBR with 4000 kmol h^{-1}. Figure 8d shows

Table 2. Reboiler and Condenser Heat Duties of C_3 Splitter (200 Stages) for the System in Figure 2b

	S/F	Reboiler (MW)	Condenser (MW)	Net Duty (MW)	Reflux Ratio
PBR	–	221	205	16	30
PBMR	1	186	172	14	25
	2	164	152	12	22
	3	150	139	10	20

Table 3. Heating and Cooling Duties for Feed/Sweep and Retentate/Permeate Streams for the System in Figure 2b

		Heating (MW)		Cooling (MW)	
	S/F	Feed	Sweep	Retentate	Permeate
PBR	–	169	–	106	–
PBMR	1	146	16	90	42
	2	126	63	78	82
	3	110	92	69	123

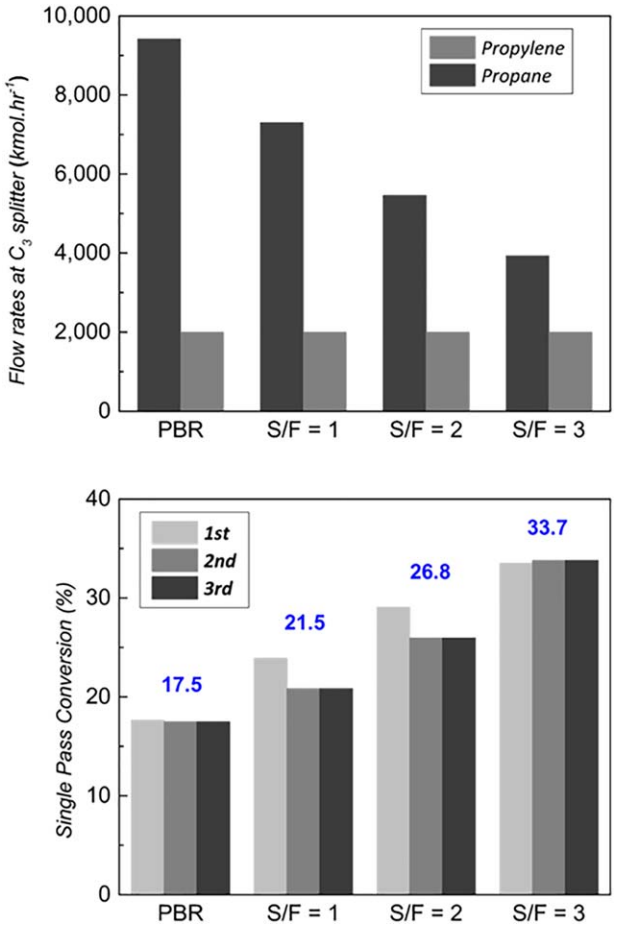

Figure 10. (a) Flow rates entering C_3 splitter and (b) single-pass conversions for the reactors-in-parallel system shown in Figure 2c.

The numbers in each condition indicate the overall single-pass conversion. [Color figure can be viewed at wileyonlinelibrary.com]

the single-stage conversions and the total conversion for each case, with S/F = 1. Due to the same propylene production rate coupled with higher conversion in the PBMR, the feed to the C_3 splitter now has considerable lower propane flow (Figure 8e) thereby resulting in considerable energy savings in the splitter even with the moderate S/F value (S/F = 1), Figure 8f). Additionally, the other energy duties do not increase significantly in comparison to the PBR (Figure 8f), since the PBMR processes a much lower feed flow rate than the PBR.

Next, we add a simple recycle to the system (Figure 2b). In this configuration, the outlet stream of propane from the bottom of the C_3 splitter is recycled and added to the fresh propane feed to the reactor, and the combined feed is then preheated to 650°C. As practically all the unreacted propane is

Table 4. Reboiler and Condenser Heat Duties of C_3 Splitter (200 Stages) for the System in Figure 2c

	S/F	Reboiler (MW)	Condenser (MW)	Net duty (MW)	Reflux Ratio
PBR	–	507	470	37	70
PBMR	1	400	371	30	55
	2	322	298	24	44
	3	251	232	19	34

Table 5. Heating and Cooling Duties for Feed/Sweep and Retentate/Permeate Streams for the System in Figure 2c

		Heating (MW)		Cooling (MW)	
	S/F	Feed	Sweep	Retentate	Permeate
PBR	–	283	–	182	–
PBMR	1	205	32	158	113
	2	165	63	127	227
	3	131	95	101	342

recycled, ~100% overall propane conversion is achieved at steady state and hence more propylene can be produced with a lower feed flow rate. The fresh propane flow rate is 4000 kmol h^{-1} in the "no-recycle" system, but here it is fixed at 2000 kmol h^{-1} in the recycled system, which corresponds to more than 600 kTA of propylene production for the same PDH plant. The required recycle flow of propane depends on the S/F ratio for both the PBR and PBMR (Figure 9a). The single-pass conversions of each reactor stage, and the total single-pass conversion of the reactor, are plotted in Figure 9b. From these figures, it is clear that the recycle flow in the PBMR is always lower than that of the PBR due to higher conversion and decreases with increased S/F. The differences in propane recycle rate have a large effect on the energy requirements of the C_3 splitter (Table 2). The reflux ratio (and hence the reboiler, condenser, and net energy duties) decrease when moving from a PBR to PBMRs with progressively higher S/F ratios. Conversely, the PBMRs use considerable amounts of sweep gas leading to other energy loads as discussed earlier. As seen in Table 3, the heating and cooling loads for the feed and retentate (propylene-rich product from the reactor) decrease as S/F increases, due to the decreasing propane flow in the system. The heating and cooling loads for the sweep and membrane permeate streams increase as expected. The overall energy loads for the C_3 splitter and the other heat exchange processes are expressed as the simple summation of absolute values of heating and cooling duties, and are shown in Figure 9c as a function of the S/F ratio. There is clearly a trade-off relationship between the two types of energy loads to be considered when using a PBMR. The overall energy load (summation of the C_3 splitter and other energy loads) is also shown in Figure 9c. It initially decreases with increasing S/F ratio but levels off at *ca.* S/F = 2, indicating that very high sweep flows do not have an overall energy saving benefit although they increase the single-pass conversion of the PBMR. In Figure 9d, we plot the total net duty, which is difference between heating and cooling energy loads. This quantity is significant for system optimization especially when heat integration is considered in the process design. The net duty changes from positive (net heating load) to negative (net cooling load) in the range of S/F = 1–1.5. Based on Figures 9c–d the optimal S/F for energy savings is around 1.5 for the PBMR system considered here. However, as discussed in previous sections, the S/F also affects the size and capital cost of the PBMR, and therefore, the optimal S/F may shift to higher values when the overall cost of the PDH plant is considered. However, a general conclusion is that hollow fiber PBMRs can create large energy savings in PDH production (e.g., ~10% saving compared to the PBR in the case of S/F = 2).

Finally, we examine a configuration in which the reactor stages are operated in parallel (Figure 2c). The first stage receives fresh (make-up) propane, whereas the propane recycled from the bottoms from the C_3 splitter is distributed

equally to the second and third reactor stages. The product streams from the three stages are combined and sent to the separation system. The potential advantage of this arrangement is that pure propane feeds enter all three reactor stages (assuming essentially perfect separation in the C_3 splitter). As shown in Figure 10a, the propane flow rate at the C_3 splitter inlet (which is the same as the propane recycle flow rate) decreases substantially in the PBMRs compared with the PBR. The energy duties for C_3 splitter and the other processes are summarized in Tables 4-5. Although the same trends are observed as in the case of a simple recycle, it is found that carrying out product separation at each reactor stage requires more energy for both C_3 splitter and other process streams than the reactors-in-series case (Tables 2-3). Unlike the simple recycled system where propane/propylene separation takes place only after three sequential PDH stages, the product separation in the parallel system leads to an increased propane flow rate at the C_3 splitter (Figure 10a). The single-pass conversion in the parallel system is shown in Figure 10b. Compared to Figure 9b, each of the single-pass conversions at the same S/F is higher than that of the simple recycled system. However, the overall single-pass conversion is much lower due to the increased amount of recycled propane from the C_3 splitter. Overall, it is found that operating the PBMRs in series results in greater energy savings than operating them in parallel, assuming the same number of PBMR units is used in each case.

Conclusions

A detailed modeling analysis of membrane reactor systems for PDH has been performed by developing a 2-D nonisothermal reactor model of PDH PBMRs and then integrating it with ASPEN process simulations of the overall PDH process including downstream separations. Several insights are obtained from this study. First, the PBMR model shows how the Péclet numbers for mass and heat transport determine the radial dispersion, relative contribution of membrane permeation, and temperature profiles of the PBMR. The sweep-to-feed (S/F) ratio is also found to be an important parameter affecting the PBMR performance. Second, it is found that PBMRs incorporating H_2-selective ceramic hollow fiber membranes with catalyst located on the shell side, are likely to be the only viable means for scale-up of PDH membrane reactors. The hollow fiber configuration minimizes radial dispersion, and increases the membrane surface area to catalyst volume ratio, thus leading to a greater enhancement effect of the membrane. The shell-side catalyst placement is necessary to facilitate regeneration/replacement and to avoid the difficulty of packing the catalyst into large numbers of fibers of small ($\sim$0.5 mm) diameter. Third, hollow fiber PBMRs also allow a large reduction in reactor volume, which becomes even smaller than the volume of a conventional PBR for the same target propylene production. Alternatively, replacement of a PBR with a PBMR containing the same amount of catalyst can lead to a large increase in propylene production (up to 45% increase) from the same PDH plant. Hollow fiber PBMRs enhance PDH conversion not only by hydrogen removal but also by providing effective heat exchange via preheated sweep gas flow in the fibers. In comparison, conventional tubular membranes will require prohibitively large reactor volumes and capital cost. Fourth, the ASPEN-based PDH process simulations incorporating the PBMR model show that a PDH system based on PBMRs in series with propane recycle from the C_3 splitter is the most effective. As the S/F value changes, a trade-off is found between energy savings at the C_3 splitter and other process energy loads (heating and cooling of the feed, sweep, permeate, and retentate). The overall energy load initially decreases with increasing S/F, and then levels off (or slowly increases). An optimal S/F ratio for energy savings is suggested to lie around 1.5 for PDH PBMRs. PBMR stages in parallel are found to be less efficient than the series configuration. Overall, this study clarifies the required process configurations and membrane characteristics for viable application to PDH PBMRs. Given existing literature demonstrations of hollow fiber ceramic membranes for separation processes, it appears quite feasible to achieve attractive energy savings at low capital cost in PDH, if hollow fiber PBMRs with high durability and good performance are developed.

Acknowledgments

This work was supported by the Dow Chemical Company.

Literature Cited

1. Tan S, Briones Gil L, Subramanian N, Sholl DS, Nair S, Jones CW, Moore JS, Liu Y, Dixit RS, Pendergast JG. Catalytic propane dehydrogenation over In2O3-Ga2O3 mixed oxides. *Appl Catal A*. 2015; 498:167–175.
2. Sattler JJHB, Ruiz-Martinez J, Santillan-Jimenez E, Weckhuysen BM. Catalytic dehydrogenation of light alkanes on metals and metal oxides. *Chem Rev*. 2014;114(20):10613–10653.
3. Weckhuysen BM, Schoonheydt RA. Alkane dehydrogenation over supported chromium oxide catalysts. *Catal Today*. 1999;51(2):223–232.
4. Gascon J, Tellez C, Herguido J, Menendez M. Propane dehydrogenation over a Cr_2O_3/Al_2O_3 catalyst: transient kinetic modeling of propene and coke formation. *Appl Catal A*. 2003;248(1–2):105–116.
5. Kumar MS, Hammer N, Ronning M, Holmen A, Chen D, Walmsley JC, Oye G. The nature of active chromium species in Cr-catalysts for dehydrogenation of propane: new insights by a comprehensive spectroscopic study. *J Catal*. 2009;261(1):116–128.
6. Iglesias-Juez A, Beale AM, Maaijen K, Weng TC, Glatzel P, Weckhuysen BM. A combined in situ time-resolved UV-Vis, Raman and high-energy resolution X-ray absorption spectroscopy study on the deactivation behavior of Pt and Pt-Sn propane dehydrogenation catalysts under industrial reaction conditions. *J Catal*. 2010;276(2): 268–279.
7. Baek J, Yun HJ, Yun D, Choi Y, Yi J. Preparation of highly dispersed chromium oxide catalysts supported on mesoporous silica for the oxidative dehydrogenation of propane using CO_2: insight into the nature of catalytically active chromium sites. *ACS Catal*. 2012;2(9): 1893–1903.
8. Wu RX, Xie PF, Cheng YH, Yue Y, Gu S, Yang W, Miao C, Hua W, Gao Z. Hydrothermally prepared Cr_2O_3-ZrO_2 as a novel efficient catalyst for dehydrogenation of propane with CO_2. *Catal Commun*. 2013; 39:20–23.
9. Jablonski EL, Castro AA, Scelza OA, de Miguel SR. Effect of Ga addition to Pt/Al_2O_3 on the activity, selectivity and deactivation in the propane dehydrogenation. *Appl Catal A*. 1999;183(1):189–198.
10. Bhasin MM, McCain JH, Vora BV, Imai T, Pujado PR. Dehydrogenation and oxydehydrogenation of paraffins to olefins. *Appl Catal A*. 2001;221(1–2):397–419.
11. Zhang YW, Zhou YM, Qiu AD, Wang Y, Xu Y, Wu PC. Propane dehydrogenation on PtSn/ZSM-5 catalyst: effect of tin as a promoter. *Catal Commun*. 2006;7(11):860–866.
12. Lobera MP, Tellez C, Herguido J, Menendez M. Transient kinetic modelling of propane dehydrogenation over a Pt-Sn-K/Al_2O_3 catalyst. *Appl Catal A*. 2008;349(1–2):156–164.
13. Li Q, Sui ZJ, Zhou XG, Zhu Y, Zhou JH, Chen D. Coke formation on Pt-Sn/Al_2O_3 catalyst in propane dehydrogenation: coke characterization and kinetic study. *Top Catal*. 2011;54(13–15):888–896.
14. Sun PP, Siddiqi G, Vining WC, Chi MF, Bell AT. Novel Pt/Mg(In)(Al)O catalysts for ethane and propane dehydrogenation. *J Catal*. 2011;282(1):165–174.
15. Vora BV. Development of dehydrogenation catalysts and processes. *Top Catal*. 2012;55(19–20):1297–1308.

16. Alcantara-Avila JR, Gomez-Castro FI, Segovia-Hernandez JG, Sotowa K, Horikawa T. Optimal design of cryogenic distillation columns with side heat pumps for the propylene/propane separation. *Chem Eng Process*. 2014;82:112–122.
17. van Miltenburg A, Zhu W, Kapteijn F, Moulijn JA. Adsorptive separation of light olefin/paraffin mixtures. *Chem Eng Res Design*. 2006; 84(A5):350–354.
18. Liao B, Lei ZG, Xu Z, Zhou RQ, Duan ZT. New process for separating propylene and propane by extractive distillation with aqueous acetonitrile. *Chem Eng J*. 2001;84(3):581–586.
19. Sirkar KK, Shanbhag PV, Kovvali AS. Membrane in a reactor: a functional perspective. *Ind Eng Chem Res*. 1999;38(10):3715–3737.
20. Coronas J, Santamaria J. State-of-the-art in zeolite membrane reactors. *Top Catal*. 2004;29(1–2):29–44.
21. McLeary EE, Jansen JC, Kapteijn F. Zeolite based films, membranes and membrane reactors: progress and prospects. *Microporous Mesoporous Mater*. 2006;90(1–3):198–220.
22. Basile A, editor. *Handbook of Membrane Reactors Volume 2: Reactor Types and Industrial Applications Preface. Reactor Types and Industrial Applications,* Woodhead Publishing Cambridge, UK 2013.
23. Kim SJ, Yang SW, Reddy GK, Smirniotis P, Dong JH. Zeolite membrane reactor for high-temperature water-gas shift reaction: effects of membrane properties and operating conditions. *Energy Fuels*. 2013; 27(8):4471–4480.
24. Kim SJ, Xu Z, Reddy GK, Smirniotis P, Dong JH. Effect of pressure on high-temperature water gas shift reaction in microporous zeolite membrane reactor. *Ind Eng Chem Res*. 2012;51(3):1364–1375.
25. Tang Z, Kim SJ, Reddy GK, Dong JH, Smirniotis P. Modified zeolite membrane reactor for high temperature water gas shift reaction. *J Membr Sci*. 2010;354(1–2):114–122.
26. Zhang YT, Wu ZJ, Hong Z, Gu XH, Xu NP. Hydrogen-selective zeolite membrane reactor for low temperature water gas shift reaction. *Chem Eng J*. 2012;197:314–321.
27. Galuszka J, Giddings T, Iaquaniello G. Membrane assisted WGSR - experimental study and reactor modeling. *Chem Eng J*. 2012;213: 363–370.
28. Chein RY, Chen YC, Chung JN. Sweep gas flow effect on membrane reactor performance for hydrogen production from high-temperature water-gas shift reaction. *J Membr Sci*. 2015;475:193–203.
29. Champagnie AM, Tsotsis TT, Minet RG, Webster IA. A high-temperature catalytic membrane reactor for ethane dehydrogenation. *Chem Eng Sci*. 1990;45(8):2423–2429.
30. Gobina E, Hughes R. Ethane dehydrogenation using a high-temperature catalytic membrane reactor. *J Membr Sci*. 1994;90(1–2): 11–19.
31. Gobina E, Hou K, Hughes R. Ethane dehydrogenation in a catalytic membrane reactor coupled with a reactive sweep gas. *Chem Eng Sci*. 1995;50(14):2311–2319.
32. van den Bergh J, Gucuyener C, Gascon J, Kapteijn F. Isobutane dehydrogenation in a DD3R zeolite membrane reactor. *Chem Eng J*. 2011;166(1):368–377.
33. Wieland S, Melin T, Lamm A. Membrane reactors for hydrogen production. *Chem Eng Sci*. 2002;57(9):1571–1576.
34. Yu W, Ohmori T, Yamamoto T, Endo A, Nakaiwa A, Itoh N. Optimal design and operation of methane steam reforming in a porous ceramic membrane reactor for hydrogen production. *Chem Eng Sci*. 2007;62(18–20):5627–5631.
35. Bernardo P, Barbieri G, Drioli E. Evaluation of membrane reactor with hydrogen-selective membrane in methane steam reforming. *Chem Eng Sci*. 2010;65(3):1159–1166.
36. Caravella A, Di Maio FP, Di Renzo A. Computational study of staged membrane reactor configurations for methane steam reforming. I. Optimization of stage lengths. *AlChE J*. 2010;56(1):248–258.
37. Saric M, van Delft YC, Sumbharaju R, Meyer DF, de Groot A. Steam reforming of methane in a bench-scale membrane reactor at realistic working conditions. *Catal Today*. 2012;193(1):74–80.
38. Di Marcoberardino G, Sosio F, Manzolini G, Campanari S. Fixed bed membrane reactor for hydrogen production from steam methane reforming: experimental and modeling approach. *Int J Hydrogen Energy*. 2015;40(24):7559–7567.
39. Patrascu M, Sheintuch M. On-site pure hydrogen production by methane steam reforming in high flux membrane reactor: experimental validation, model predictions and membrane inhibition. *Chem Eng J*. 2015;262:862–874.
40. Ziaka ZD, Minet RG, Tsotsis TT. Propane dehydrogenation in a packed-bed membrane reactor. *AlChE J*. 1993;39(3):526–529.
41. Ziaka ZD, Minet RG, Tsotsis TT. A high-temperature catalytic membrane reactor for propane dehydrogenation. *J Membr Sci*. 1993; 77(2–3):221–232.
42. Collins JP, Schwartz RW, Sehgal R, Ward TL, Brinker CJ, Hagen GP, Udovich CA. Catalytic dehydrogenation of propane in hydrogen permselective membrane reactors. *Ind Eng Chem Res*. 1996;35(12): 4398–4405.
43. Weyten H, Keizer K, Kinoo A, Luyten J, Leysen R. Dehydrogenation of propane using a packed-bed catalytic membrane reactor. *AlChE J*. 1997;43(7):1819–1827.
44. Weyten H, Luyten J, Keizer K, Willems L, Leysen R. Membrane performance: the key issues for dehydrogenation reactions in a catalytic membrane reactor. *Catal Today*. 2000;56(1–3):3–11.
45. Kotanjac ZS, Annaland MV, Kuipers JAM. Demonstration of a packed bed membrane reactor for the oxidative dehydrogenation of propane. *Chem Eng Sci*. 2010;65(22):6029–6035.
46. Teixeira M, Madeira LM, Sousa JM, Mendes A. Improving propyne removal from propylene streams using a catalytic membrane reactor-a theoretical study. *J Membr Sci*. 2011;375(1–2):124–133.
47. Shelepova EV, Vedyagin AA, Mishakov IV, Noskov AS. Mathematical modeling of the propane dehydrogenation process in the catalytic membrane reactor. *Chem Eng J*. 2011;176:151–157.
48. Didenko LP, Savchenko VI, Sementsova LA, Chizhov PE, Bykov LA. Dehydrogenation of propane in a combined membrane reactor with hydrogen-permeable palladium module. *Petrol Chem*. 2013; 53(1):27–32.
49. Choi SW, Jones CW, Nair S, Sholl DS, Moore JS, Liu Y, Dixit RS, Pendergast JG. Material properties and operating configurations of membrane reactors for propane dehydrogenation. *AlChE J*. 2015; 61(3):922–935.
50. Kim SJ, Liu Y, Moore JS, Dixit RS, Pendergast JG, Sholl DS, Jones CW, Nair S. Thin hydrogen-selective SAPO-34 zeolite membranes for enhanced conversion and selectivity in propane dehydrogenation membrane reactors. *Chem Mater*. 2016;28(12):4397–4402.
51. Tsai CY, Ma YH, Moser WR, Dixon AG. Modeling and simulation of a nonisothermal catalytic membrane reactor. *Chem Eng Commun*. 1995;134:107–132.
52. Chan PPY, Vanidjee K, Adesina AA, Rogers PL. Modeling and simulation of non-isothermal catalytic packed bed membrane reactor for H_2S decomposition. *Catal Today*. 2000;63(2–4):379–385.
53. Jeong BH, Sotowa KI, Kusakabe K. Modeling of an FAU-type zeolite membrane reactor for the catalytic dehydrogenation of cyclohexane. *Chem Eng J*. 2004;103(1–3):69–75.
54. Kumar S, Gaba T, Kumar S. Simulation of catalytic dehydrogenation of cyclohexane in zeolite membrane reactor. *Int J Chem Reactor Eng*. 2009;7:A13.
55. Daramola MO, Burger AJ, Giroir-Fendler A. Modelling and sensitivity analysis of a nanocomposite MFI-alumina based extractor-type zeolite catalytic membrane reactor for *m*-xylene isomerization over Pt-HZSM-5 catalyst. *Chem Eng J*. 2011;171(2):618–627.
56. Casanave D, Ciavarella P, Fiaty K, Dalmon JA. Zeolite membrane reactor for isobutane dehydrogenation: experimental results and theoretical modelling. *Chem Eng Sci*. 1999;54(13–14):2807–2815.
57. Gobina E, Hou K, Hughes R. Mathematical-analysis of ethylbenzene dehydrogenation - comparison of microporous and dense membrane systems. *J Membr Sci*. 1995;105(3):163–176.
58. Koukou MK, Papayannakos N, Markatos NC. Dispersion effects on membrane reactor performance. *AlChE J*. 1996;42(9):2607–2615.
59. Gobina E, Hou K, Hughes R. Equilibrium-shift in alkane dehydrogenation using a high-temperature catalytic membrane reactor. *Catal Today*. 1995;25(3–4):365–370.
60. Ciavarella P, Casanave D, Moueddeb H, Miachon S, Fiaty K, Dalmon JA. Isobutane dehydrogenation in a membrane reactor - influence of the operating conditions on the performance. *Catal Today*. 2001;67(1–3):177–184.
61. Gallucci F, De Falco M, Tosti S, Marrelli L, Basile A. Co-current and counter-current configurations for ethanol steam reforming in a dense Pd-Ag membrane reactor. *Int J Hydrogen Energy*. 2008; 33(21):6165–6171.
62. Dowling AW, Vetukuri SRR, Biegler LT. Large-scale optimization strategies for pressure swing adsorption cycle synthesis. *AlChE J*. 2012;58(12):3777–3791.
63. Couck S, Gobechiya E, Kirschhock CEA, et al. Adsorption and separation of light gases on an amino-functionalized metal-organic framework: an adsorption and in situ XRD study. *ChemSusChem*. 2012;5(4):740–750.

64. Ribeiro AM, Grande CA, Lopes FVS, Loureiro JM, Rodrigues AE. A parametric study of layered bed PSA for hydrogen purification. *Chem Eng Sci*. 2008;63(21):5258–5273.
65. Zhu JW, Guo SB, Liu GP, Liu ZK, Zhang ZC, Jin WQ. A robust mixed-conducting multichannel hollow fiber membrane reactor. *AlChE J*. 2015;61(8):2592–2599.
66. Rahman MA, Garcia-Garcia FR, Hatim MDI, Kingsbury BFK, Li K. Development of a catalytic hollow fibre membrane micro-reactor for high purity H_2 production. *J Membr Sci*. 2011;368(1–2):116–123.
67. Garcia-Garcia FR, Rahman MA, Gonzalez-Jimenez ID, Li K. Catalytic hollow fibre membrane micro-reactor: high purity H_2 production by WGS reaction. *Catal Today*. 2011;171(1):281–289.
68. Czuprat O, Schiestel T, Voss H, Caro J. Oxidative coupling of methane in a BCFZ perovskite hollow fiber membrane reactor. *Ind Eng Chem Res*. 2010;49(21):10230–10236.
69. Wu ZT, Hatim IMD, Kingsbury BFK, Gbenedio E, Li K. A novel inorganic hollow fiber membrane reactor for catalytic dehydrogenation of propane. *AlChE J*. 2009;55(9):2389–2398.
70. Israni SH, Nair BKR, Harold MP. Hydrogen generation and purification in a composite Pd hollow fiber membrane reactor: experiments and modeling. *Catal Today*. 2009;139(4):299–311.
71. Gimeno MP, Wu ZT, Soler J, Herguido J, Li K, Menendez M. Combination of a two-zone fluidized bed reactor with a Pd hollow fibre membrane for catalytic alkane dehydrogenation. *Chem Eng J*. 2009; 155(1–2):298–303.
72. Xu X, Yang W, Liu J, Lin L, Stroh N, Brunner H. Synthesis of NaA zeolite membrane on a ceramic hollow fiber. *J Membr Sci*. 2004; 229(1–2):81–85.
73. Kingsbury BFK, Li K. A morphological study of ceramic hollow fibre membranes. *J Membr Sci*. 2009;328(1–2):134–140.
74. Xu G, Wang K, Zhong Z, Chen C-S, Webley PA, Wang H. SiC nanofiber reinforced porous ceramic hollow fiber membranes. *J Mater Chem A*. 2014;2(16):5841–5846.

Manuscript received Jan. 25, 2017, and revision received Mar. 21, 2017.